Spectra of $K\alpha$ x rays from 64-MeV sulfur ions traveling in solids

R. L. Watson, J. R. White, A. Langenberg, R. A. Kenefick, and C. C. Bahr
Cyclotron Institute, Texas A&M University, College Station, Texas 77843
(Received 19 February 1980)

Spectra of $K\alpha$ x rays from 64-MeV sulfur ions incident on a wide range of thick elemental targets have been measured with a plane crystal spectrometer. Various features of the spectra were found to be sensitive to the atomic structure of the targets. In particular, the $K\alpha$ satellite and hypersatellite intensity distributions displayed oscillatory variations $\sim 14\%$ as a function of target atomic number. This behavior is satisfactorily accounted for by the systematics of electron-capture cross sections. Considerable line broadening was observed, and the Lorentzian component of the total linewidth was found to increase linearly with the product of the target atomic number and the atomic concentration.

I. INTRODUCTION

Recently, it has been recognized that high-resolution investigations of K x rays emitted during the passage of energetic heavy ions through material media are capable of providing information relating to the charge-state equilibration process.[1-7] The competition between electron ionization, excitation, capture, and decay quickly leads to the establishment of an equilibrium distribution of excited states in the moving projectile. Many of these excited states have x ray decay branches and hence their populations may be estimated from measured x ray intensities. Bell *et al.*[8] and Schule *et al.*[9] have utilized high-resolution measurements of the spectra of K x rays emitted by sulfur and neon ions to estimate the average projectile charges inside target foils.

Owing to the complexity of the spectrum of x rays emitted from a multielectron heavy ion, it is generally not possible to determine the population of each of the many x-ray-emitting states available to the projectile. Also some states are produced which do not have x-ray decay branches. These two problems greatly limit the applicability of x-ray spectroscopy to the direct determination of charge states. On the other hand, it is reasonable to expect that the integrated intensities of $K\alpha$ x-ray satellites and hypersatellites from the various states belonging to a particular K-L vacancy configuration will give an approximate representation of the relative contribution of that configuration to the distribution of K-L vacancy configurations in the beam. Thus it is possible that projectile x-ray spectra could be quite useful for elaborating general trends in the K- and L-shell ionization and capture cross sections as a function of such parameters as target atomic number and projectile velocity.

In the present investigation, the spectra of $K\alpha$ satellite and hypersatellite x rays emitted from 64-MeV (incident energy) sulfur ions moving in solids have been measured for a wide range of thick elemental targets. The primary objective of this study was to ascertain the extent to which various features of the x-ray relative intensity distributions and peak widths could be understood in terms of the systematics of cross sections for K- and L-shell ionization, excitation, and capture. This study is an extension of an earlier investigation of the $K\alpha$ hypersatellite to satellite yield ratio as a function of target atomic number.[10]

II. EXPERIMENTAL METHODS

A beam of 64-MeV S^{4+} ions was extracted from the Texas A & M variable-energy cyclotron, directed through a 3-mm-diameter collimator located 30 cm in front of the target position and focused on various targets positioned at 45° with respect to the beam axis. The spectra of K x rays emitted by the S ions were measured using a plane crystal spectrometer which had been mounted on a turntable, thus enabling it to be positioned at any observation angle between 162 and 20° with respect to the beam axis. In this study, most of the measurements were performed at an observation angle of 90°, however, several spectra were also recorded at an observation angle of 135° in order to determine the average projectile energy for x-ray emission inside the target by measuring x-ray Doppler shifts. Details of the spectrometer alignment procedures will be given in a forthcoming paper on x-ray energy shifts in solid targets.[11]

The spectra of sulfur $K\alpha$ satellite and hypersatellite x rays were measured for a wide range of thick elemental targets using a NaCl crystal and a flow proportional counter employing a 90% argon–10% methane gas mixture. The spectrometer resolution at 2460 eV was 6.9 eV full width at half maximum (FWHM) as determined from spectra obtained using a thin (8 $\mu g/cm^2$) carbon

foil. The counting time at each spectrometer position was regulated by monitoring the number of particles scattered at 45° from a thin gold foil (mounted over the collimator) into a surface barrier detector. Spectra for several of the targets were repeated using a germanium (111) crystal. Since the reflectivity of germanium is nearly constant over the range of wavelengths spanned by the sulfur $K\alpha$ satellites and hypersatellites,[12] comparison of the two sets of spectra enabled the determination of reflectivity corrections for the NaCl crystal. It was found that the reflectivity of the NaCl crystal for 2620-eV x rays was a factor of 1.50 ± 0.12 lower than for 2460-eV x rays.

A comparison of spectra obtained with a number of different targets using the NaCl crystal is shown in Fig. 1. The energy scales in the figure have been corrected for Doppler shift which at 90° causes the observed energies to be approximately 5 eV lower than the emitted energies. The most prominent set of peaks on the left-hand side of each spectrum includes, in order of increasing energy,

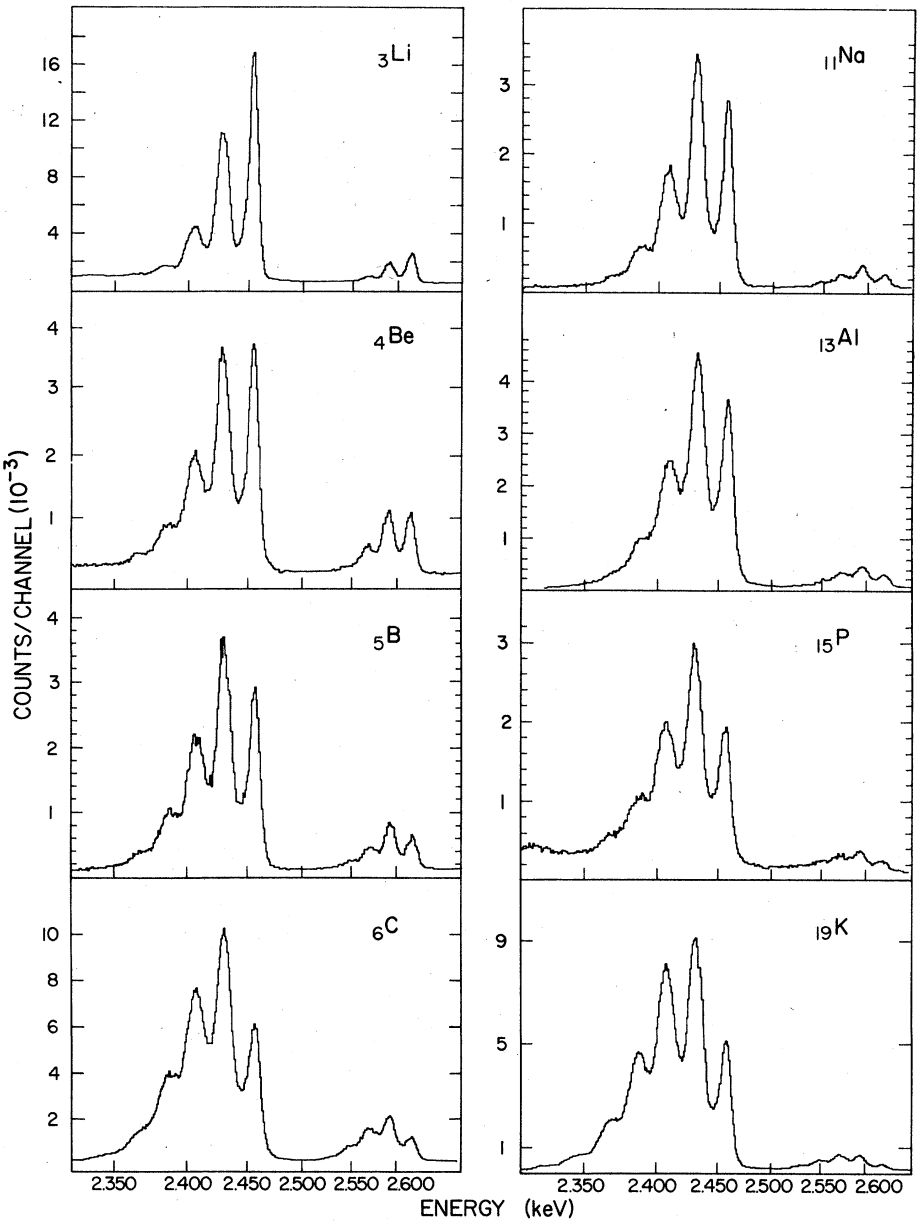

FIG. 1. Spectra of $K\alpha$ x-rays emitted in various thick solid targets by 64-MeV (incident energy) sulfur ions.

the satellite groups resulting from $K\alpha$ x-ray emission from initial states having a single K vacancy and 3, 4, 5, 6, and 7 L vacancies, respectively (i. e., the KL^3, KL^4, KL^5, KL^6, and KL^7 satellite groups). The low-intensity set of peaks on the right-hand side of each spectrum includes (in order of increasing energy), the hypersatellite groups resulting from $K\alpha$ x-ray emission from initial states having a double K vacancy and 4, 5, 6, and 7 L vacancies, respectively (i. e., the K^2L^4, K^2L^5, K^2L^6, and K^2L^7 hypersatellite groups). The highest intensity satellite and hypersatellite peaks in the spectrum for a Li target are, respectively, the heliumlike sulfur $2^1P \rightarrow 1^1S$ transition and the hydrogenlike sulfur $2^2P \rightarrow 1^2S$ transition.

The spectra were analyzed by means of a least-squares-fitting program employing Voigt functions. In this way, integrated intensities were obtained for each of the satellite and hypersatellite groups. An example of how the x-ray structure was fitted is shown in Fig. 2. Each x-ray group was represented by a single Voigt function, even though some of the weaker lines of a given configuration lie in the regions of the satellite groups on either side. To some extent, these contributions tend to cancel and the minor errors introduced by this approximate representation of the group intensities are not expected to have a significant effect on the results presented here. The small peak between the KL^6 and KL^7 satellite groups in Fig. 2 approximately accounts for some high energy components of KL^6 and for the $KL^7\ ^3P \rightarrow {}^1S$ transition, which in solid targets contributes very little intensity because of its relatively long (metastable) radiative lifetime. A detailed discussion of the multiplet structure comprising these spectra will be presented elsewhere.[13]

As already mentioned, measurements were also performed at an observation angle of 135° to determine the average projectile energy for x-ray emission from the observed x-ray Doppler shift. The average projectile energy loss in a carbon target (high stopping power, low x-ray absorption coefficient) was found to be 5.5 ± 0.5 MeV while the average energy loss in a silicon target (low stopping power, high x-ray absorption coefficient) was found to be 4.2 ± 0.5 MeV. Using the stopping power tables of Northcliffe and Schilling,[14] these energy losses translate into average depths for x-ray emission of 0.29 mg/cm^2 and 0.28 mg/cm^2 in carbon and silicon, respectively. Based upon these results, average depths for x-ray emission were estimated for the other targets and used to correct the x-ray relative intensities for absorption. These corrections generally changed the relative intensities by less than 15% and were rather insensitive to errors in the estimated average x-ray emission depths. For example, the correction factor for the observed ratio of the intensity of the $K^2L^7(^2P)$ peak to the intensity of the $KL^7(^1P)$ peak in a silicon target was 0.93, assuming an effective thickness of 0.28 mg/cm^2 for both x-ray transitions (as indicated above). This correction factor would change by only 5% for a factor of 2 increase in the effective thickness. The small differences in average x-ray emission depths due to different thickness dependences of the emission rates of the various x-ray lines were neglected. Corrections were also applied to the relative intensities for absorption in the proportional counter window, for the efficiency of the proportional counter, and for the reflectivity of the crystal.

III. RESULTS AND DISCUSSION

A. The satellite and hypersatellite intensity distributions

It is evident in Fig. 1 that considerable variation occurs in the distribution of L-shell vacancies present at the time of K x-ray emission. This may be shown more directly by using the satellite and hypersatellite relative intensities to calculate approximate average L-vacancy fractions:

$$\bar{p}_L = \tfrac{1}{8} \sum n f_n , \qquad (1)$$

where n is the number of missing L electrons and

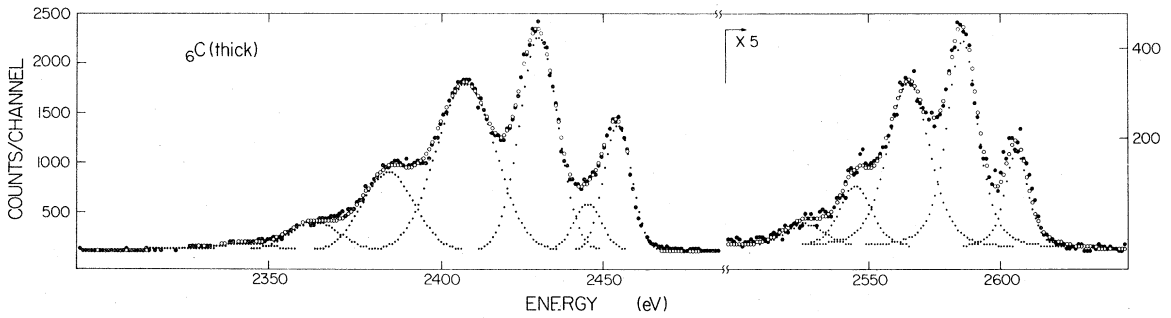

FIG. 2. A sulfur-ion $K\alpha$ x-ray spectrum, obtained with a thick carbon target, showing the results of a least-square peak-fitting analysis. The filled circles are the data points and the open circles are the calculated points.

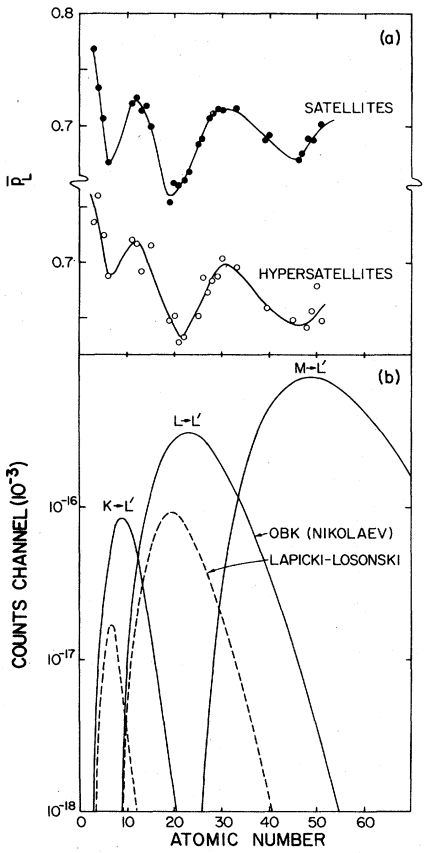

FIG. 3. (a) The dependence of the approximate average L-vacancy fraction $\bar{p}_L$ on target atomic number. (b) Cross sections for the capture of an electron from the K, L, and M shell of the target to the L shell of a 60-MeV sulfur ion. The solid curves were calculated using the OBK formula of Nikolaev and the dashed curves were calculated using the prescription of Lapicki and Losonsky.

f_n is the relative intensity of the corresponding satellite or hypersatellite group. Since the fluorescence yield has not been taken into account in the calculation of $\bar{p}_L$, this parameter will only be used as a *relative* measure of the average number of L-shell vacancies associated with each x-ray distribution.

A graph of $\bar{p}_L$ versus target atomic number is presented in Fig. 3a for the satellite and the hypersatellite x-ray groups. It is seen that in both cases, the relative degree of L-shell ionization exhibits an oscillatory behavior with minima near $Z=6$, 18, and 43. It is interesting to note that the average of the K-binding energies for C and N ($Z=6$ and 7) is 347 eV, the average of the L-binding energies for Cl–K ($Z=17$–19) is 333 eV, and the average of the M-binding energies for Nb–Ru ($Z=41$–44) is 331 eV. Thus, the observed minima all occur in regions where the average binding energies of target K-, L-, or M-shell electrons are nearly the same. The average L-binding energy of a neutral sulfur atom is about half of this value while the average L-binding energy of a Li-like sulfur ion (the most probable ion state associated with K x-ray emission) is approximately twice this value.

The close correspondence of the $\bar{p}_L$ values for the satellites with those of the hypersatellites is rather remarkable, considering the multiplet structure comprising the two distributions is quite different. The satellite and hypersatellite distributions observed with thin targets, for example (where most of the x-ray emission occurs outside the target), look very different because of the presence of additional intense peaks in the satellite distribution resulting from metastable transitions. The fact that the satellite and hypersatellite relative intensity distributions are essentially identical in thick targets indicates that the equilibrium distribution of L-shell vacancies is independent of the number of K-shell vacancies.

The influence of projectile energy loss on the satellite and hypersatellite structure was checked by measuring additional spectra for 32- and 105-MeV sulfur ions in Li, B, Al, and Ca targets. It was found that $d\bar{p}_L/dE$ was nearly the same for all of the materials, with an average value of $4.6 \times 10^{-3}\,\mathrm{MeV}^{-1}$. Since the average energy loss in the target also does not vary substantially among the various targets, the $\bar{p}_L$ changes due to projectile energy loss will not significantly alter the structural features displayed in Fig. 3(a).

A similar oscillatory behavior has previously been observed in the dependence of the equilibrium K-vacancy bearing fractions of sulfur- and chlorine-ion beams on target atomic number.[15-17] These effects have generally been ascribed to electron capture from the target to the projectile K shell. A qualitative explanation of the $\bar{p}_L$ oscillations may be given in terms of the relative importance of electron capture in determining the equilibrium distribution of L-shell vacancies in the beam. When electron capture is relatively more important than ionization, $\bar{p}_L$ should decrease whereas when electron capture is relatively less important than ionization, $\bar{p}_L$ should increase. Since it is expected that the L-shell ionization cross sections for sulfur ions will increase smoothly with increasing target atomic number, the observed minima in the $\bar{p}_L$ curves should correspond to maxima in cross sections for capture from different target shells to the projectile L shell.

In order to test this hypothesis, cross sections for electron capture to the L shell of sulfur have been computed using the Oppenheimer-Brinkmann-Kramer (OBK) formula as given by Nikolaev (including screening),[18] and using the prescription

given recently by Lapicki and Losonsky.[19] The calculated cross sections for capture to the L shell of the sulfur ion from the K shell of the target ($K \rightarrow L'$), the L shell of the rarget ($L \rightarrow L'$), and the M shell of the target ($M \rightarrow L'$; OBK only) are shown in Fig. 3(b). An average projectile energy of 60 MeV and an average sulfur L-shell binding energy of 632 eV (estimated for Li-like sulfur ions) were used in the calculations. A comparison of Figs. 3 (a) and 3(b) shows that the observed minima do indeed correlate with predicted maxima in the electron-capture cross sections. The maxima for the OBK cross sections, however, appear to be shifted up by about 4 atomic number units from the $\bar{p}_L$ minima, whereas the Lapicki-Losonsky cross section maxima for K- and L-electron capture coincide almost exactly with the $\bar{p}_L$ minima.

B. The intensity ratio of ^2P to ^1P

The relative yields of sulfur ions having double and single K vacancies may be examined by comparing the intensity of $K\alpha$ x rays arising from the $^2P \rightarrow {}^2S$ transition (K^2L^7 peak) with the intensity of $K\alpha$ x rays arising from the $^1P \rightarrow {}^1S$ transition (KL^7 peak). Assuming the equilibrium distribution of L-shell vacancies is established very quickly (i. e., within the first few $\mu g/cm^2$) and that this distribution is independent of the number of K-shell vacancies, the number of x rays from state j of an electron configuration having k K-shell vacancies and n L-shell vacancies, escaping through the front surface of the target is given by

$$N_j = N_p \int_0^t G_j P_n \sigma_{Rj} Y_k e^{-c\sigma_A x} dx , \tag{2}$$

where N_p is the number of incident ions; Y_k the fraction of ions having k K-shell vacancies; P_n the fraction of ions having n L-shell vacancies; G_j the probability that an ion having k K-shell vacancies and n L-shell vacancies will be in state j; σ_{Rj} the cross section for radiative decay from state j, $(nv\tau_{Rj})^{-1}$ where n is the number of target atoms/cm^3, v is the ion velocity, and τ_{Rj} is the mean lifetime for radiative decay; x the depth in target in units of atoms/cm^2; $e^{-c\sigma_A x}$ the x-ray absorption correction, where cx is the x-ray path length and σ_A is the x-ray-absorption cross section; and t the effective thickness for x-ray emission in a thick target.

Since the average energy loss was found to be fairly small (~5 MeV), the variation of P_n, σ_{Rj}, and Y_k with projectile velocity will be neglected. Furthermore, because Y_k reaches its equilibrium value within approximately the first 150 $\mu g/cm^2$, the fraction of ions having k K-shell vacancies will be treated as a constant. Applying the above approximations, Eq. (2) reduces to

$$N_j \cong (N_p G_j P_n Y_{k\infty} / nv\tau_{Rj})\, T_j , \tag{3}$$

where

$$T_j = (1/c\sigma_A)(1 - e^{-c_A t}) ,$$

$Y_{k\infty}$ is the equilibrium fraction of ions having k K-shell vacancies. This last equation may then be used to express the ratio of the intensities of the $^2P/^1P$ transitions. The result is

$$R_{2P/1P} = N_2 T_1 / N_1 T_2 = G_2 \tau_{R1} Y_{2\infty} / G_1 \tau_{R2} Y_{1\infty} . \tag{4}$$

(Quantities subscripted by the number 2 refer to the ^2P state while those subscripted by the number 1 refer to the ^1P state.)

According to the three-component model for predicting the K-vacancy distribution of an ion beam,[20] the ratio of the equilibrium double K-vacancy fraction to the equilibrium single K-vacancy fraction is given by[10,21]

$$\frac{Y_{2\infty}}{Y_{1\infty}} = \frac{\sigma_{10}\sigma_{02} + \sigma_{12}\sigma_{01} + \sigma_{12}\sigma_{02}}{\sigma_{20}\sigma_{01} + \sigma_{21}\sigma_{01} + \sigma_{21}\sigma_{02}} . \tag{5}$$

In the above equation, the quantities σ_{ij} are total cross sections for producing j K vacancies in an ion initially having i K vacancies. Since none of the cross sections appearing in Eq. (5) has yet been measured for the systems under consideration, it is necessary to make further approximations; namely, it will be assumed that σ_{02} and σ_{21} are approximately negligible,

$$\sigma_{01} \approx \sigma_{I(K)} ,$$

$$\sigma_{12} \approx \tfrac{1}{2}\sigma_{01} ,$$

$$\sigma_{10} = \sigma_{C(K)} + \sigma_D ,$$

$$\sigma_{21} \simeq 2\sigma_{10} ,$$

where $\sigma_{I(K)}$ is the cross section for K shell ionization (excitation is neglected), $\sigma_{C(K)}$ is the cross section for capture to the K-shell, and σ_D is the cross section for radiative decay. Under these conditions

$$Y_{2\infty}/Y_{1\infty} \approx \sigma_{01}/4\sigma_{10} . \tag{6}$$

The final result is obtained by using statistical population probabilities for G_1 and G_2 and theoretical mean lifetimes for τ_1 (1.49×10^{-14} sec) (Ref. 22) and τ_2 (2.44×10^{-14} sec) (Ref. 23),

$$R_{2P/1P} \approx 0.61\sigma_{I(K)}/(\sigma_{C(K)} + \sigma_D) . \tag{7}$$

The experimental intensity ratios are shown in Fig. 4 plotted versus target atomic number. As in the case of the total hypersatellite to satellite yield ratio,[10] an oscillatory structure is observed. According to Eq. (7), the minima should correspond to maxima in cross sections for electron capture

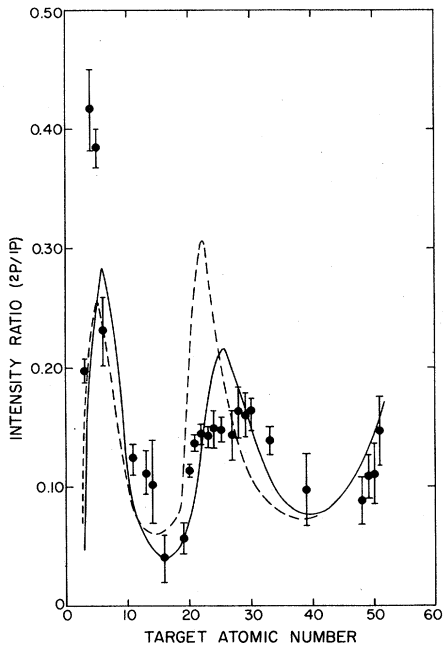

FIG. 4. The ratio of the intensity of the $2^2P \rightarrow 1^2S$ transition to the intensity of the $2^1P \rightarrow 1^1S$ transition are as a function of target atomic number. The solid curve was calculated using OBK K-capture cross sections and the dashed curve was calculated using Lapicki-Losonsky K-capture cross sections.

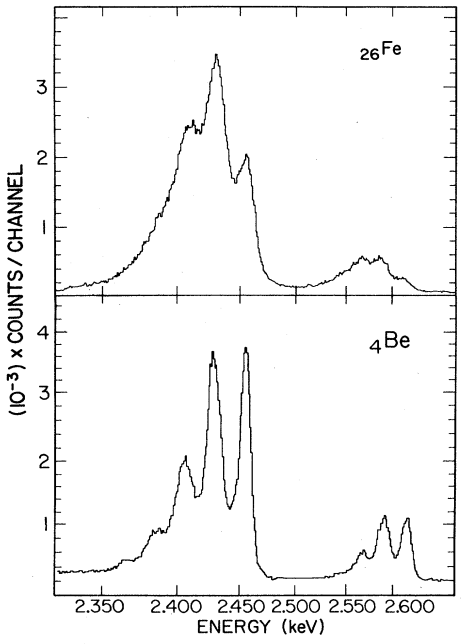

FIG. 5. A comparison of sulfur-ion $K\alpha$ x-ray spectra, obtained with an Fe and a Be target, showing the effect of line broadening.

to the projectile K shell. The solid line in Fig. 4 shows the ratios calculated with Eq. (7) using K-ionization cross sections obtained from the binary encounter approximation (BEA)[24] and total K-capture cross sections calculated using the OBK formula given by Nikolaev.[18] These latter cross sections were multiplied by a scaling factor of 0.34 as indicated by the recent work of Chan and Eichler.[25] The cross section for decay was calculated using an average K-vacancy lifetime of 1.5×10^{-14} sec as measured by Betz *et al.*[26] The dashed curve in Fig. 4 was calculated in a similar manner except that the total K-capture cross sections used were those computed with the Lapicki-Losonsky[19] prescription.

It is apparent that both calculated curves in Fig. 4 reproduce the main features of the measured $^2P/^1P$ intensity ratios rather well. The results obtained using scaled OBK K-capture cross sections appear to give a better representation of the data in the region around $Z = 20$–30. In any case, the close correspondence between the experimental and predicted ratios is deemed to be somewhat remarkable in view of the number of simplifying approximations and assumptions employed.

C. Line broadening

As a consequence of the multiple collisions suffered by an ion as it moves in a solid and the large cross sections associated with collisional excitation and decay processes, a considerable amount of line broadening is to be expected. Such broadening effects have been observed previously for $K\alpha$ x rays from 90-keV Ne and 1-MeV B projectiles,[6] and 4-MeV Ne (Ref. 27). In each of these cases, however, the broadening was so severe that the discrete satellite structure was no longer observable and hence accurate values of individual linewidths could not be obtained.

In the present study, the effects of line broadening did not totally obscure the $K\alpha$ satellite structure even in the worst cases, as may be seen in Fig. 5 where spectra obtained using Fe and Be targets are compared. It is readily apparent that the structure in the Fe spectrum is much broader than that in the Be spectrum, but the major peaks in the satellite region are still discernable. As in the previous cases mentioned above, Doppler broadening accounts for only a small part of the total peak width. The total peak width (FWHM) predicted for the ^1P peak in the Fe spectrum (Fig. 5) by combining in quadrature the spectrometer resolution (6.9 eV), the Doppler broadening due to projectile energy loss (0.7 eV), the Doppler broadening due to the angular divergence of the spectrometer soller slits (0.9 eV), and the esti-

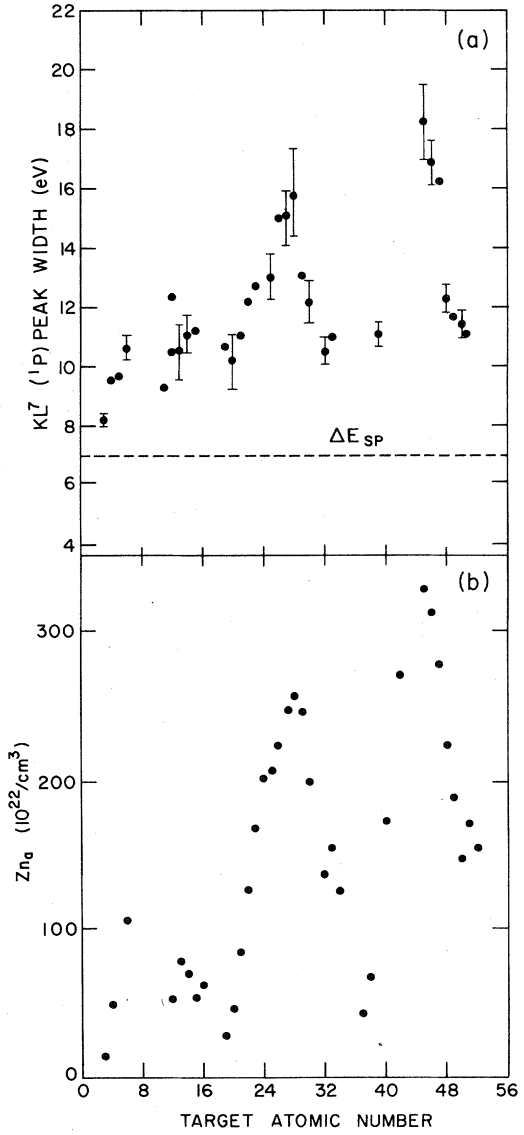

FIG. 6. (a) The total width (FWHM) of the ^1P peak as a function of target atomic number. The dashed line indicates the spectrometer resolution. (b) The product of the target atomic number and atomic concentration plotted versus target atomic number.

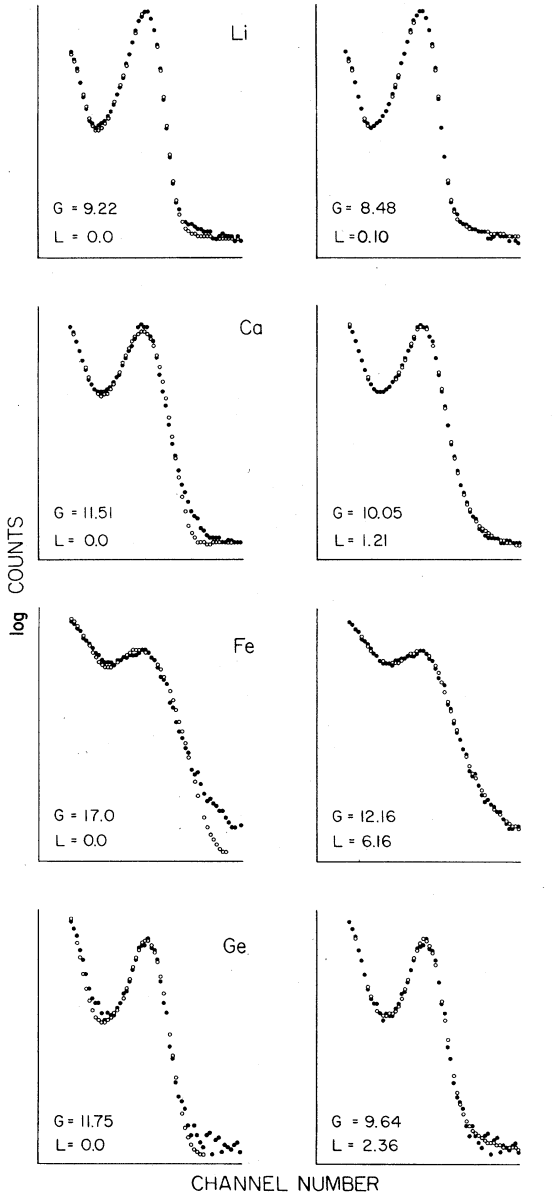

FIG. 7. A comparison of least-squares fits to the ^1P peak for a series of different targets. The left-hand side of the figure shows the results of using a Gaussian peak shape, while the right-hand side shows the fits obtained with a Voigt function. The numbers labeled G and L are, respectively, the Gaussian and Lorentzian widths (in channels) at half maximum points.

mated Doppler broadening due to multiple scattering (≈2.0 eV) is 7.3 eV. The measured total width is 15.0 eV.

The behavior of the total width of the ^1P (KL^7) satellite peak as a function of target atomic number is shown in Fig. 6(a). The dashed line indicates the spectrometer resolution. Overall, the widths increase steadily with increasing atomic number. However, two regions stand out quite clearly where the widths rise dramatically above the general trend. The structural features in Fig. 6(a) are remarkably similar to those displayed by the graph of Z times the atomic concentration n_a, versus Z shown in Fig. 6(b).

A careful analysis of the ^1P peak in each of the spectra was performed using both Gaussian line shapes and Voigt profiles (i. e., convoluted Gaussian and Lorentzian functions), in an effort to distinguish between broadening associated with lifetime shortening effects and broadening arising

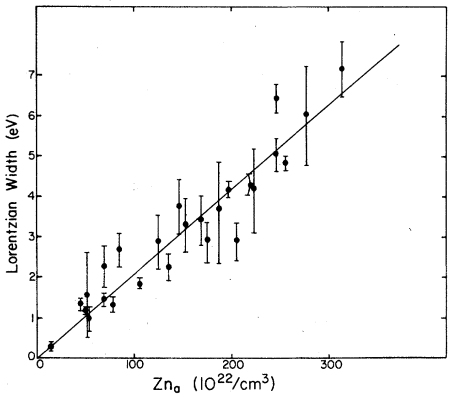

FIG. 8. The Lorentzian width (FWHM) of the ^1P peak as a function of the product of the target atomic number and the atomic concentration. The solid line shows the best linear fit to the data for an intercept fixed at zero.

from other sources (e. g., Doppler-shift effects). A definite Lorentzian broadening component was found, as is illustrated in Fig. 7. In Fig. 7, some fits obtained for the ^1P peak using Gaussian line shapes (left-hand side of the figure) are compared with the fits obtained with Voigt line shapes (right-hand side of the figure). The best Gaussian and Lorentzian widths are given by the least-squares-fitting procedure are listed in the lower left-hand corner of each spectrum. The Gaussian fits deviate significantly from the observed shapes in the regions of the peak tails and maxima. Because of the structural similarities displayed by Figs. 6(a) and 6(b), the dependence of the Lorentzian width on Zn_a was investigated. As shown in Fig. 8, the Lorentzian width was found to be directly proportional to Zn_a. The straight line shows the best linear fit to the data points for an intercept fixed at zero. The slope of this line is $(2.17 \pm 0.08) \times 10^{-24}$ eV cm^3.

Baranger[28] has derived a result, which appears to be of general applicability to the present problem, from a theoretical analysis of pressure broadening in optical spectra. Pressure broadening is caused by the interactions (elastic and inelastic) of light emitting atoms, molecules, or ions with the constituents of their environment (usually a gas). The following formula gives the energy width (FWHM) of an isolated line resulting from the interactions with perturbers of density n per unit volume,

$$\Gamma = \tfrac{1}{2}\hbar(nv\sigma)_{\mathrm{av}}. \tag{8}$$

Here σ is the total interaction cross section and v is the perturber velocity, over which σ must be averaged. Presumably, in the present case, the dominant contributions to σ come from the cross sections for capture and loss of L electrons.

Experimentally, it was found that $\Gamma = kZn_a$, where k is a proportionality constant (see Fig. 8). Combining this result with Eq. (8) gives

$$\sigma/Z = 2k/\hbar v \tag{9}$$

and since v is, in this case, the projectile velocity, Eq. (9) predicts that σ/Z is a constant. Setting k equal to the slope of the line in Fig. 8, yields the value 3.47×10^{-18} cm^2 for σ/Z. The sum $(\sigma_{C(L)} + \sigma_{C(K)} + \sigma_{I(L)} + \sigma_{I(K)})/Z$, where σ_C is the OBK electron-capture cross section (multiplied by 0.34) and σ_I is the BEA ionization cross section, ranges from 3.0×10^{-18} cm^2 at $Z = 3$ to 4.8×10^{-17} cm^2 at $Z = 50$. Thus, the value of σ/Z deduced from the experimental ^1P peak widths is of the order of magnitude predicted for collisional broadening due to K- and L-electron capture and ionization. The fact that the theoretical cross sections overestimate σ/Z at high Z do not account for its linear dependence on Zn_a should not be regarded as particularly significant since the theories on which they are based are being applied far outside their expected regions of validity.

IV. CONCLUSIONS

Various features of the spectrum of $K\alpha$ x rays emitted by 64-MeV sulfur ions moving in solids have been found to undergo considerable change as the target atomic number is varied. A detailed examination of the Z dependence of the $K\alpha$ satellite and hypersatellite relative intensity distributions has shown that the observed structural changes are associated with electron capture to the projectile L shell from near-lying levels of the target. An analysis of the $^2P/^1P$ intensity ratio using the three-component model for projectile K-vacancy formation yielded surprisingly good agreement with the experimental results. The broadening of the ^1P line was studied and it was found that the Lorentzian width is directly proportional to the product of the target atomic number and the atomic concentration. This observation leads to the conclusion that the total cross section for depopulating the ^1P state depends linearly on target Z. The magnitude of this cross section supports the hypothesis that collisional ionization and capture of K- and L-electrons is the dominant broadening mechanism.

ACKNOWLEDGMENTS

We thank J. McCalpin, K. Wittnebel, and S. Merritt for helping with the experiments. We are grateful to D. A. Church and J. F. Reading for helpful discussions. This work was supported by the U. S. Department of Energy under contract DE-AS05-78ER06036 and by the Robert A. Welch Foundation.

[1]C. F. Moore, H. H. Wolter, R. L. Kauffman, J. McWherter, J. E. Bolger, and C. P. Browne, J. Phys. B 5, L262 (1972).
[2]A. R. Knudson, P. G. Burkhalter, and D. J. Nagel, Phys. Rev. A 10, 2118 (1974).
[3]H. Panke, F. Bell, H.-D. Betz, W. Stehling, E. Spindler, and R. Laubert, Phys. Lett. 53A, 457 (1975); H. Panke, F. Bell, H.-D. Betz, and W. Stehling, Nucl. Instrum. 132, 25 (1976).
[4]D. L. Matthews, R. J. Fortner, and G. Bissinger, Phys. Rev. Lett. 36, 664 (1976).
[5]R. J. Fortner and D. L. Matthews, Phys. Rev. A 16, 1441 (1977).
[6]R. J. Fortner, D. L. Matthews, J. D. Garcia, and H. Oona, Phys. Rev. A 14, 1020 (1976).
[7]C. L. Cocke, *Beam Foil Spectroscopy*, edited by I. A. Sellin and D. J. Pegg (Plenum, New York, 1976), Vol. I, p. 283.
[8]F. Bell, H. D. Betz, H. Panke, W. Stehling, and E. Spindler, J. Phys. B 9, 3017 (1976).
[9]R. Schule, H. Stafast, and K. Bethge, Z. Phys. A 291, 117 (1979).
[10]R. L. Watson, J. R. White, and F. E. Jenson, Phys. Lett. 67A, 269 (1978).
[11]R. L. Watson, A. Langenberg, J. R. White, R. A. Kenefick, C. C. Bahr, and J. McCalpin (unpublished).
[12]G. Brogren and E. Hörnström, Ark. Fys. 23, 81 (1962).
[13]A. Langenberg, R. L. Watson, and J. R. White, J. Phys. B (in press).
[14]L. C. Northcliffe and R. F. Schilling, Nucl. Data Tables A 7, 233 (1970).
[15]F. Hopkins, J. Sokolov, and A. Little, Phys. Rev. A 15, 588 (1977).
[16]C. L. Cocke, S. L. Varghese, and B. Curnutte, Phys. Rev. A 15, 874 (1977).
[17]T. J. Gray, C. L. Cocke, and R. K. Gardner, Phys. Rev. A 16, 1907 (1977).
[18]V. S. Nikolaev, Zh. Eksp. Teor. Fiz. 51, 1263 (1966) [Sov. Phys.—JETP 24, 847 (1967)].
[19]G. Lapicki and W. Losonsky, Phys. Rev. A 15, 896 (1977).
[20]R. K. Gardner, T. J. Gray, P. Richard, C. Schmiedekamp, K. A. Jamison, and J. M. Hall, Phys. Rev. A 15, 2202 (1977).
[21]S. K. Allison, Rev. Mod. Phys. 30, 1137 (1958).
[22]C. D. Lin, W. R. Johnson, and A. Dalgarno, Phys. Rev. A 15, 154 (1977).
[23]H. A. Bethe and E. E. Salpeter, *Quantum Mechanics of One- and Two-Electron Atoms* (Springer, Berlin, 1958), p. 265.
[24]J. S. Hansen, Phys. Rev. A 8, 822 (1973).
[25]F. T. Chan and J. Eichler, Phys. Rev. Lett. 42, 58 (1979).
[26]H.-D. Betz, F. Bell, H. Panke, G. Kalkoffen, M. Wely, and D. Evers, Phys. Rev. Lett. 33, 807 (1974).
[27]F. Hopkins, *Proceedings of Fourth International Conference on Science and Industrial Applications of Small Accelerators* (North Texas State University, Denton, Texas, 1976), p. 37.
[28]M. Baranger, Phys. Rev. 111, 481 (1958); 112, 855 (1958).